

seg_3D_by_PC2D: Multi-View Projection for Domain Generalization and Adaptation in 3D Semantic Segmentation

Andrew Caunes^{1,2}, Thierry Chateau¹, Vincent Frémont²

Abstract—3D semantic segmentation plays a pivotal role in autonomous driving and road infrastructure analysis, yet state-of-the-art 3D models are prone to severe domain shift when deployed across different datasets. We propose a novel multi-view projection framework that excels in both domain generalization (DG) and unsupervised domain adaptation (UDA). Our approach first aligns Lidar scans into coherent 3D scenes and renders them from multiple virtual camera poses to create a large-scale synthetic 2D dataset (PC2D). We then use it to train a 2D segmentation model in-domain. During inference, the model processes hundreds of views per scene; the resulting logits are back-projected to 3D with an occlusion-aware voting scheme to generate final point-wise labels. Our framework is modular and enables extensive exploration of key design parameters, such as view generation optimization (VGO), visualization modality optimization (MODO), and 2D model choice. We evaluate on the nuScenes and SemanticKITTI datasets under both the DG and UDA settings. We achieve state-of-the-art results in UDA and close to state-of-the-art in DG, with particularly large gains on large, static classes. Our code and dataset generation tools will be publicly available at <https://github.com/andrewcaunes/ia4markings>.

I. INTRODUCTION

3D semantic segmentation of Lidar scenes is crucial for applications such as autonomous driving (AD) and road infrastructure analysis. In particular, many applications require models to be able to generalize to unseen data, which may not be from the same *domain* as the training data, e.g. if the data was acquired in a different location or with a different sensor. The main attempts to mitigate this problem are *Domain Generalization* (DG) and *Unsupervised Domain Adaptation* (UDA).

Most existing methods are tailored for AD, thus making concessions on accuracy to guarantee real-time performance on single or few scans.

We propose a method that leverages aligned scenes and larger computation times to perform 3D semantic segmentation. In particular, it reaches state-of-the-art-level performance in domain generalization and unsupervised domain adaptation. It is particularly effective on static classes, but can also be close to state-of-the-art on dynamic classes.

Our method belongs to the multi-view projection family, where 3D scenes are analyzed via multiple 2D representations. We position virtual cameras around aligned Lidar scenes to generate rendered views from various perspectives. The key innovation is our approach to 2D model training. While usual methods use camera images for training and inference [1], we create large-scale synthetic datasets by

rendering both the 3D scenes and their corresponding ground truth annotations. This enables the 2D segmentation model to be trained on data closely matching the inference domain, allowing to freely choose the optimal features for the views. The extensive use of 2D models leads to interesting domain adaptation performance. We demonstrate the effectiveness of our method for domain generalization and unsupervised domain adaptation on the nuScenes [2] and SemanticKITTI [3] datasets. We also conduct an ablation study to verify the importance of each component of our method. **Our main contributions are:**

- A novel modular multi-view projection framework with dataset generation capabilities that can be used to explore many approaches and parameters
- A state-of-the-art method for domain generalization and domain adaptation, especially interesting for static or large classes

II. RELATED WORKS

A. 3D semantic segmentation

3D semantic segmentation is the task of assigning a semantic label to each point in a 3D pointcloud. It is generally done either on Lidar pointclouds [2], [3], or RGB-D images [4]. Methods are usually divided in 3D-based and 2D-based. 3D models directly operate on the pointcloud using 3D sparse convolutions [5], while 2D models re-use 2D image segmentation methods by projecting the pointcloud to a 2D plane [6]. 3D models generally achieve higher accuracy while being slower and more memory consuming. Importantly, 3D models have been shown to suffer from domain shift

to a higher degree than 2D models [7]. 2D approaches generally project the pointcloud to a single 2D image with channels representing various features, e.g. height (in Bird’s Eye View), intensity, density, etc. Multi-view projection methods try to leverage 2D models even further by repeatedly using the same model on multiple views of the same 3D scene.

B. Multi-view projection for segmentation

The goal of multi-view projection methods is to extract as much knowledge from a 2D model as possible for 3D segmentation. This is done by inferring on multiple views of the 3D scene and then merging the resulting 2D segmentations. The problem then decomposes itself into two parts:

- 1) Which views to use for inference
- 2) How to merge the 2D segmentation masks to get unique 3D labels

¹Logiroad

²LS2N - Ecole Centrale de Nantes

Notice that the second problem is equivalent to the 2D-3D label propagation problem [8]. It is generally solved using either a voting scheme [9]–[11], where either the 2D masks or the probabilities/logits of the model are accumulated on points as votes, or with more complex methods such as Neural Networks [12]–[14]. Our proposed method uses a simple voting scheme on accumulated logits from a single 2D model.

In this paper, we focus on the first problem. Initially, [15] proposed multi-view projection for indoor RGB-D scenes, where the views are simply the RGB-D images themselves. For outdoor Lidar scenes, the same reasoning led [1] to use aligned RGB camera images as views, for which 2D annotated data is available [16]. This approach is limited however as it requires using additional sensors, and the performance is tied to the quality of the sensor alignment. Mitigating this, [11] proposed to infer on rendered views of 3D scenes with an out-of-domain 2D model trained on camera images. This has the advantage of not requiring 3D labels or additional sensors, but comes with several limitations:

- The domain gap between camera images and views of Lidar pointclouds is substantial, which negatively impacts 2D model performance.
- The multi-view aspect of the method is limited because the view generation method must align with the camera images, e.g., be from a road user’s perspective.
- Because aligning Lidar scans is essential for obtaining dense 3D scenes, the method is limited to static classes, as dynamic classes often appear with a so-called ‘shadow effect’ in the aligned scene, which is wildly out of the camera images’ domain.

We propose to solve all of these limitations by leveraging 3D annotations. This makes our method more dependent on 3D annotated data, but allows to reach significantly better performance. Closest to our approach, [9] proposes to use 3D annotations to generate 2D synthetic datasets to train a 2D model for downstream multi-view projection for indoor RGB-D scenes. Our method distinguishes itself in its application to outdoor Lidar scenes, where much additional processing is required to obtain satisfying views, e.g. scan aligning and meshing, as well as in the choices for the feature rendering and view selection. Furthermore, we demonstrate the potential of such methods for domain generalization and unsupervised domain adaptation.

C. Domain Generalization and Domain Adaptation

Domain generalization (DG) and Unsupervised Domain Adaptation (UDA) have the same goal of adapting a model trained on samples (X_S, Y_S) from a domain (distribution) \mathcal{D}_S to infer on samples X_T from a different target domain \mathcal{D}_T , for which no label is available. The difference is that in UDA, unlabeled feature samples from the target domain $X_{T,train}$ are available for adaptation, while in DG, even the features of the target domain are unknown at adaptation time [17]. Note that for UDA, $X_{T,train}$ is different from $X_{T,test}$, which is the set of samples used for evaluation. This

nuance is rarely mentioned in UDA literature, but the choice of whether to use $X_{T,test}$ for adaptation is important and depends on the application. Post-processing methods may assume $X_{T,test}$ is available at adaptation time, while real-time applications such as AD shouldn’t. We use this latter configuration to compare our method to the state of the art UDA methods which we assume did the same.

Recent domain adaptation methods leverage temporal coherence and self-training. T-UDA [18] combines sequential pointcloud consistency and cross-sensor geometric alignment within a mean-teacher self-ensembling framework, effectively using temporal cues to guide the model’s adaptation. Similarly, Lidar-UDA [19] adopts a two-stage self-training strategy that simulates differing Lidar scan patterns via random beam dropping and enforces cross-frame consistency by ensembling predictions from consecutive frames, yielding more reliable pseudo-labels.

As a more recent field, DG for Lidar semantic segmentation has only recently begun to take shape. [20] laid some foundations, introducing an approach in which augmented pointcloud is obtained and constraints on the model’s features are applied to ensure internal feature alignment. [21] obtained state-of-the-art results by learning a density discriminative feature embedding to facilitate the segmentation of objects with same densities across sensors. Very closely, [22] learns a common density-agnostic embedding for 3D pointclouds, based on occupancy information from sparse convolutions and voxel density prediction.

III. METHOD

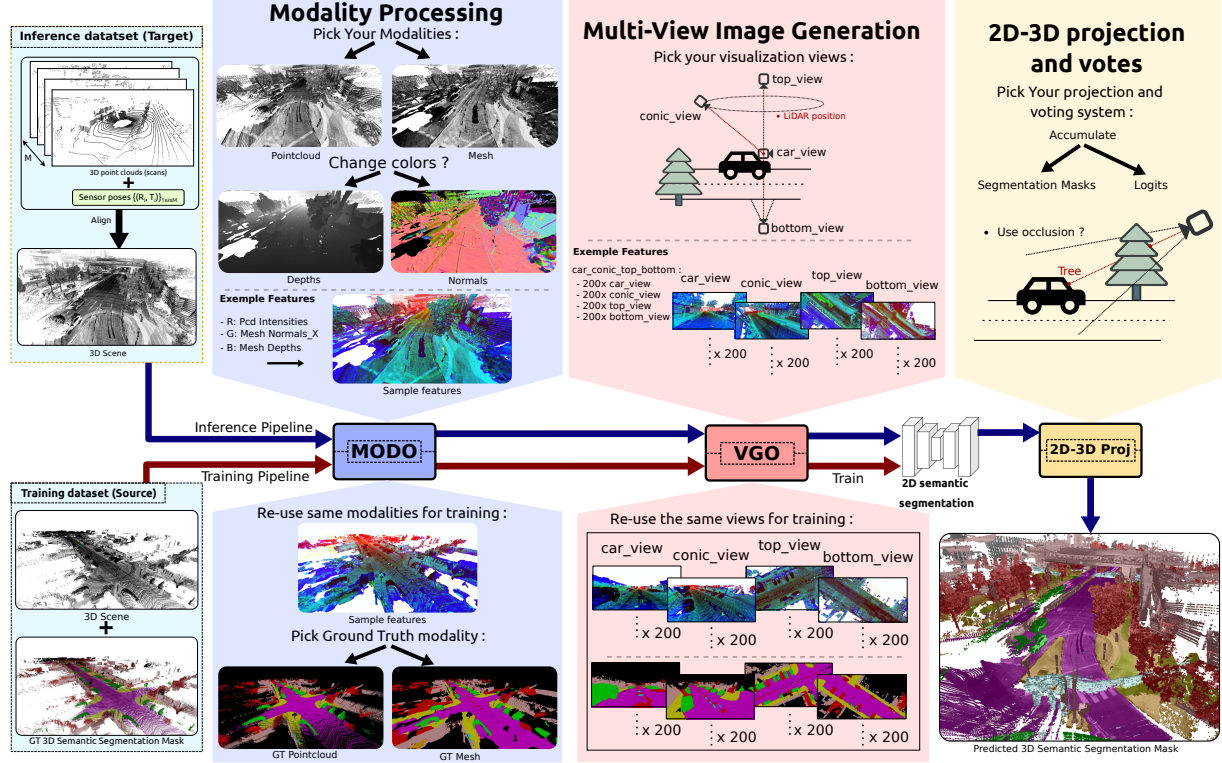
A. Base method

An overview of our method is shown in Figure 1. We propose to enhance and extend the 3D Multi-View Projection method used in [11]. This base method proposes to do multi-view projection of 2D segmentation masks on 3D pointclouds by inferring on views of 3D scenes with a 2D model trained on camera images. Here, we refer to *scenes* as the concatenation of multiple Lidar scans aligned in a common reference frame. Our key innovation is to re-train the 2D model in-domain. First, we use 3D annotations to generate a large-scale synthetic dataset of views of 3D scenes along with 2D segmentation masks, which we use to train the 2D model. Second, we optimize parameters such as visualization modalities (MODO) (III-D) and view generation method (VGO) (III-C) to obtain the best performance. At the cost of requiring 3D supervision, this approach remedies all the limitations of the base method, and achieves state-of-the-art performance in the domain generalization setting. Lastly, we improve the base method’s projection by adding occlusion using depth maps (OCL) (III-F).

B. Training in-domain using 3D annotations in 2D (PC2D)

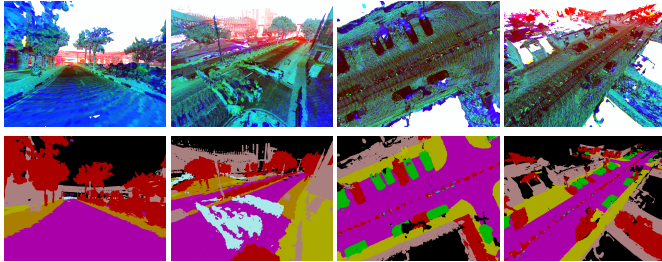
In [11], the domain of the generated views must be as close as possible to the domain of the camera training images. The main extension we propose to the base method is to train the 2D model in-domain using 3D annotations. To this end, we generate a large-scale synthetic dataset of views of

Fig. 1: Overview of the framework.



3D scenes along with 2D segmentation masks. This is done by applying the same steps required to generate views for inference, i.e. generating virtual camera poses and rendering views, but using both the 3D scene and the 3D semantic segmentation mask as inputs. We can generate an arbitrary number of (image, label) pairs, e.g. as many as there are training iterations. Training on such a synthetic dataset can be seen as a kind of powerful data augmentation. The only limitation is that a limited number of annotated scenes will lead to samples with less diversity as the total number of training samples increases. We show samples of such a dataset in Figure 2.

Fig. 2: PC2D dataset samples showing rendered views of 3D scenes (top) configuration with their corresponding segmentation masks (bottom). Red channel is pointcloud intensities, Green channel is mesh intensities, Blue channel is depth. Generated from nuScenes [2] and SemanticKITTI [3].



The use of PC2D datasets allows to choose the domain of the training images, which allows full freedom over the view

generation steps during both training and inference. The two following subsections describe how we optimize the camera pose generation and the modality choice to obtain the best performance.

C. View Generation Optimization (VGO)

We propose to optimize the view generation by choosing relevant camera poses. In the base method, the camera poses are all placed at a road user’s perspective to match training data. We keep this category and add 3 new categories of camera poses. All 4 types of camera pose are obtained based on the original Lidar sensor poses, which are already describing the trajectory of the ego vehicle along the scene. An illustration of the 4 types of camera pose is shown in Figure 1 in the VGO module (red), and we describe them below:

- **car_view**: The camera is placed at a road user’s perspective, i.e. at the approximate height of a car, and looks around (random yaw can be applied). Can be useful to maintain compatibility of the model with potential additional camera images data.
- **conic_view**: The camera is placed on the basis of a large imaginary cone pointing downwards, with the apex at the Lidar sensor position. The camera points to the apex of the cone. This corresponds to a ‘drone’ or ‘lamp post’ view of the scene, and is also the closest to the views that a human annotator would typically use to annotate a scene, as it gives a large field of view and a ‘natural’ perspective of the scene.

- **top_view**: The camera is placed directly above the Lidar position, looking downwards, with variable height and roll. This corresponds to the usual ‘bird’s eye view’ of the scene.
- **bottom_view**: The camera is placed directly below the Lidar position, looking upwards. This is the opposite of the top view. It may appear counter-intuitive, but seeing Lidar scenes from below allows to clearly see the colors of the flat surfaces of the ground without occlusions from the objects above and less noise.

We experiment with the number of camera poses per scene and the channel configuration, and retain as best configuration to use all 4 types of camera poses, with 200 camera poses per type, per scene, thus 800 total views per scene. We call this configuration ‘*car_conic_top_bottom*’. A scene is on the order of $\sim 100\text{--}300\text{m}$ across. Using more views seems not to improve the performance, and using fewer views leads to a drop.

D. Modality Optimization (MODO)

Similar to camera pose generation, PC2D datasets allow us to choose the visualization modality for the training and inference images, i.e. it is no longer required to match the domain of camera images. Choosing a modality comes down to picking channels for the rendered images. The number of channels can be arbitrary, and we experiment with various types of channels. The various choices that are available are illustrated in Figure 1 in the MODO module (blue). A first choice to make is either to render views from pointclouds directly or rendering from generated meshes, as a mesh can make objects appear more continuous and less sparse. This choice is also applicable for the labels being generated for PC2D datasets: 2D segmentations masks viewed from Ground Truth 3D segmentation masks can be generated either from the pointcloud (‘*pff*’ as in ‘points for labels’) or from the mesh (‘*mfl*’). Then, we experiment with 3 types of channels for the features:

- **Intensities**: The Lidar sensor intensity, normalized by scan as described in [11].
- **Depths**: The pointcloud/mesh depth maps with respect to the camera pose.
- **Normals**: The components of the pointcloud/mesh normals, computed using the normal estimation method in [23].

The best MODO feature configuration for our method is called ‘*trimerge*’, as in ‘Merge 3 channels’. The features rendered using the ‘*trimerge*’ configuration can be observed in Figure 1 and Figure 2. It is described in Table I. It corresponds to using 3-channel images composed of ‘pointcloud with Lidar intensities’, ‘mesh with Lidar intensities’, and ‘depth map from mesh’. For the labels, we use the pointcloud views directly. More details can be found in IV-B.

E. 2D Model Training

For the PC2D dataset generation, we generate at least as many images as there are training iterations. For instance, for 90k training iterations with batch size 16, we generate

$\sim 1.5M$ (image, label) pairs. Experiments show that high-resolution images lead to the best results, so we use a first low-resolution training phase with 1024×512 (LD) images, and then a second high-resolution training phase with 2048×1024 (HD) images. We use 2D models out of the box as detailed in IV-B. We use few augmentations since the PC2D dataset already provides much diversity.

F. Projection and Voting

As stated in II-B, we don’t modify the projection step of the base method, which simply back-projects and accumulates the 2D logits on the points then use these as majority votes. We propose adding occlusion to the projection step. Naive back-projection from 2D to 3D suffers from points being included in the projection even if they are occluded by other points. We use depth maps generated from meshes, themselves generated using [23] for occlusion. Using meshes has the advantage of allowing less sparse depth maps which is more appropriate for dense segmentation masks. Finally, we set and tune a margin parameter δ to include points behind the depth map to account for the size of the projected object.

IV. EXPERIMENTS

In this section we demonstrate the performance of our method on Lidar Semantic Segmentation tasks. In particular, the 2D reliance of our method shows the most benefits when applied to domain adaptation. We use two datasets: nuScenes [2] (NS) and SemanticKITTI [3] (SK) on which we evaluate the 4 settings: NS \rightarrow NS, SK \rightarrow SK, NS \rightarrow SK and SK \rightarrow NS, in both the domain generalization (DG) and unsupervised domain adaptation (UDA) settings. We compare our method to the state-of-the-art methods in both settings in IV-C. We also conduct an ablation study to demonstrate the importance of each component of our method in IV-D.

A. Datasets

SemanticKITTI [3] and nuScenes [2] are two well-known large-scale datasets for AD, both providing and annotating Lidar 3D pointclouds. The procedure generally adopted in domain generalization and unsupervised domain adaptation literature [17]–[19], [21] is to train on the official training splits for both datasets, e.g. 700 scenes for nuScenes and sequences 00-07 and 09-10 for SemanticKITTI, and evaluate on the official validation splits, e.g. 150 scenes for nuScenes and sequences 08 for SemanticKITTI. We follow this procedure for comparing with the state of the art.

B. Implementation details

There are many hyper-parameters in our method that allow to try many different approaches. We present the most important ones here, and how we set them for the best performance.

1) *Dataset preparation*: To begin with, we prepare the aligned scenes from SemanticKITTI and nuScenes. We use the already existing scenes from NS and accumulate scans 100 by 100 to create SK scenes. The intensities are normalized following [11]. We crop the scenes only below the ground to remove noise, at -2.2m for SK and -2.5m for NS, with the reference being the first Lidar position for each scene. Note that we do not crop nuScenes to fit the lower height of SemanticKITTI as is often done, as this would fall outside the scope of domain generalization.

We generate meshes for each scene using [23] with the recommended parameters.

To prepare for 2D segmentation label generation for PC2D datasets, we process nuScenes annotations which are only available at 2Hz, with scans at 20Hz. We make them denser by using a simple K-Nearest Neighbors method with $K = 5$ to assign labels to each point in the scene.

We alternately use subsets or the full datasets for our experiments due to the large size of the datasets. For IV-C we use the full datasets, and for IV-D and other validation experiments, we use subsets NStr200 and NSval50 composed respectively of the 200 and 50 first and last training scenes from nuScenes.

2) *Method specific parameters*: For the VGO module, we apply random rotations and offsets to the generated camera poses for more diversity.

For the MODO module, we use either the ‘trimerge_pfl’ or the ‘trimerge_normals_XY_mfl’ as detailed in Table I. These were found to perform best after validation on NSval50. We use images of size 2048×1024 (HD) or 1024×512 (LD), depending on the experiments. The point size used for visualization is 4px in HD for pointcloud views.

TABLE I: Channel assignments for two MODO configurations.

Channel	<i>trimerge</i>	<i>trimerge_normals_XY</i>
R	pointcloud intensities	pointcloud intensities
G	mesh intensities	mesh depth
B	mesh depth	mesh normals (X)
A	–	mesh normals (Y)

For the back-projection step, we crop the projection outside a depth range of [1m, 30m], and when occlusion is used, we set the occlusion margin to $\delta = 0.5m$ behind the depth encountered. We accumulate the logits over the inference results, as it achieved better performance than accumulating the masks.

For the 2D segmentation model, we use a Mask2Former [24] model with Swin backbone [25], from the framework of [26]. We pretrain the model on the PC2D dataset for 90k iterations on LD resolution images with a batch size of 16, followed by for 30k more iterations on HD resolution images with a batch size of 4. We use a fading learning rate of $1e^{-4}$ for LD images, then $2e^{-5}$ for HD images.

For a fair comparison in UDA, we follow [18], [19] and use a MinkowskiNet 32 from [5] as the 3D segmentation model with the framework of [27]. We train it with the default settings for 3×12 epochs on the source dataset then

3×12 epochs on the target pseudo-annotated dataset with a batch size of 32.

C. Domain Generalization and Unsupervised Domain Adaptation

In this section, we test our method in the domain generalization and unsupervised domain adaptation settings and compare it to state-of-the-art methods. For DG, we use the *DGLSS* setting from [17] for the class mapping and metrics to guarantee a fair comparison. We compare our results to recently published [17] and [21]. We re-use their results directly in Table II. To also compare our method to the UDA state-of-the-art, we first train a 3D model on the source dataset, then generate pseudo-labels using our pipeline (also trained on the source dataset) on the target features and finally re-train the 3D model with these pseudo-labels. We follow [18] for the classes mapping, which include the ‘manmade’ class, but don’t account for it the *mIoU* since [19] doesn’t report it. Similarly, we don’t include the ‘other-vehicle’ class in the *mIoU* as it is not defined the same way in [18], [19]. Full details about the class mappings and metrics can be found at <https://github.com/andrewcaunes/ia4markings>. All the results are using the Intersection over Union (IoU) metric, and can be seen in Table II. The best score per experiment per task is in bold, * means classes not accounted for UDA and ** means classes not accounted for both DG and UDA in the *mIoU* calculation.

As a first observation, our method does not perform as well as 3D models on the NS \rightarrow NS and SK \rightarrow SK settings, showing the superiority of state-of-the-art 3D methods when applied in-domain. However, our method performs better than the state-of-the-art domain generalization methods in the NS \rightarrow SK for many classes, including all the static classes and the ‘car’ (+2.8) and ‘bicycle’ (+0.39) classes. The progressions in the ‘drivable’ and ‘sidewalk’ classes are significant with respectively +5.33 and +19.38 in IoU. We note that the classes where our method comes out the most are the large, static classes, while it struggles with the small, dynamic classes such as ‘pedestrian’ (-24.2). We note that our method does not stand out as much in the SK \rightarrow NS setting, where it performs below the state-of-the-art. This might be related to the difference in the height of the scenes, the densities or the intensity distributions between NS and SK.

Compared to the UDA state-of-the-art, again, our method stands out in the NS \rightarrow SK setting, where it dominates on most classes except for the pedestrian class. Notably, the ‘motorcycle’ class where the method underperforms in DG obtains an outstanding increase of +216% in IoU, which may be due to the complementary nature of source training and pseudo-labeling.

D. Ablation Study

The results of the ablation study can be seen in Table III. We start with the base method from [11] trained on camera images from the Mapillary Vistas dataset [16], then add

TABLE II: Domain Generalization and Unsupervised Domain Adaptation performance in IoU for all configurations between nuScenes and SemanticKITTI datasets. The best score per experiment per task is in bold, * means classes not accounted for UDA and ** means classes not accounted for both DG and UDA in the $mIoU$ calculation.

	car	bicycle	motorcycle	truck	o-vehicle*	pedestrian	drivable	sidewalk	walkable	vegetation	manmade**	mIoU
NS → NS												
DGLSS [17]	-	-	-	-	-	-	-	-	-	-	-	-
DDFE [21]	89.11	7.43	44.51	69.21	74.69	67.60	96.58	75.71	73.43	83.37	-	68.16
Ours (<i>trimerge-pfl</i>)	71.96	20.16	29.87	36.52	0	55.20	93.28	72.11	65.73	86.14	-	58.38
SK → SK												
DGLSS	92.76	11.99	27.09	72.50	45.95	36.39	84.76	65.64	67.98	91.28	-	59.62
DDFE	91.86	21.65	48.11	26.84	40.04	62.32	91.90	79.65	72.29	90.31	-	62.50
Ours (<i>trimerge-pfl</i>)	91.32	35.78	11.83	0.03	20.17	22.87	90.55	79.60	63.93	88.01	-	50.41
NS → SK												
DG												
DGLSS	-	-	-	-	-	-	-	-	-	-	-	-
DDFE	86.63	4.83	29.35	24.80	13.45	38.70	80.97	48.79	52.52	85.14	-	46.52
Ours (<i>trimerge-pfl</i>)	89.55	5.22	21.77	4.40	0.66	14.50	86.30	68.17	54.78	73.93	-	41.93
UDA												
T-UDA [18]	93.0	0.0	11.4	3.4	47.0	15.7	83.3	54.4	67.9	83.9	79.4	45.89
Lidar-UDA [19]	86.19	0.00	13.87	9.30	3.1	16.49	65.69	6.07	54.05	85.65	-	37.48
Ours (UDA)	91.02	0.3	43.9	16.8	0	7.86	85.1	68.1	68.3	74.3	70.8	50.63
SK → NS												
DG												
DGLSS	76.36	1.51	35.18	26.47	25.49	37.09	82.03	38.12	44.20	81.79	-	44.83
DDFE	75.29	3.84	29.28	30.11	31.37	51.69	87.85	50.02	51.10	83.77	-	49.43
Ours (<i>trimerge-normals-XY-mfl</i>)	54.34	0.47	0.46	9.65	0	6.58	85.24	48.1	37.87	78.51	-	35.59
UDA												
T-UDA	74.2	0.5	40.3	21.8	0.2	0.4	87.8	45.8	46.1	70.3	72.6	43.02
Lidar-UDA	73.48	0.85	15.86	0.9	25.67*	40.78	87.44	42.31	47.88	83.22	41.84	43.64
Ours (UDA)	67.97	0	22.47	23.7	0	3.37	89.12	55.82	56.59	80.22	78.52	44.36

components one by one. The evaluation is done in the NS → NS setting on the NSval50 dataset as described in IV-B. This experiment confirms the importance of each component, and since VGO and MODO can both be considered parameter tuning of the PC2D dataset addition, we can conclude that the inclusion of the PC2D dataset leads to a dramatic performance increase.

TABLE III: Ablation study. Semantic Segmentation on nuScenes.

Stage	Added component	mIoU
(I)	Base [11]	19.12
(II)	+ PC2D	27.18 (+42.2%)
(III)	+ VGO	41.99 (+119.6%)
(IV)	+ MODO	46.09 (+141.1%)
(V)	+ OCL	49.67 (+159.78%)

V. CONCLUSION

We have presented a novel multi-view projection framework for 3D semantic segmentation that is especially well suited for both domain generalization and unsupervised domain adaptation. By generating large-scale synthetic 2D datasets (PC2D) from aligned Lidar scenes, our method leverages occlusion-aware back-projection and voting to produce high-quality 3D labels without requiring any target features or annotations.

Extensive experiments on the nuScenes and SemanticKITTI benchmarks demonstrate that our approach achieves state-of-the-art performance in both the DG

and UDA settings. In particular, we observe dramatic gains on large, static classes—up to +19.4 mIoU on ‘sidewalk’ and +5.3 mIoU on ‘drivable’ under DG—and consistent improvements across most categories when adapting between these challenging datasets in UDA. An ablation study confirms that each component of our pipeline contributes significantly to the overall performance.

Our framework is modular and flexible: the PC2D generation can accommodate arbitrary camera poses, feature channels, 2D models, and provide many hyperparameters.

Future work will explore extending the pipeline to improve the projection step and applying it to other tasks, such as Sim-to-Real adaptation. We also plan to investigate the use of additional modalities, such as RGB imagery, within the same multi-view projection framework to further improve robustness across diverse sensor configurations.

ACKNOWLEDGMENTS

This project was provided with AI computing and storage resources by GENCI at IDRIS thanks to the grant 2024-AD011012128 on the supercomputer Jean Zay’s V100 and H100 partitions.

Large language models were used for spelling correction.

REFERENCES

- [1] K. Genova, X. Yin, A. Kundu, C. Pantofaru, F. Cole, A. Sud, B. Brewington, B. Shucker, and T. Funkhouser, “Learning 3D Semantic Segmentation with only 2D Image Supervision,” Oct. 2021, arXiv:2110.11325 [cs]. [Online]. Available: <http://arxiv.org/abs/2110.11325>

- [2] H. Caesar, V. Bankiti, A. H. Lang, S. Vora, V. E. Liong, Q. Xu, A. Krishnan, Y. Pan, G. Baldan, and O. Beijbom, "nuScenes: A multimodal dataset for autonomous driving," May 2020, arXiv:1903.11027 [cs, stat]. [Online]. Available: <http://arxiv.org/abs/1903.11027>
- [3] J. Behley, M. Garbade, A. Milioto, J. Quenzel, S. Behnke, C. Stachniss, and J. Gall, "SemanticKITTI: A Dataset for Semantic Scene Understanding of LiDAR Sequences," Aug. 2019, arXiv:1904.01416 [cs]. [Online]. Available: <http://arxiv.org/abs/1904.01416>
- [4] A. Dai, A. X. Chang, M. Savva, M. Halber, T. Funkhouser, and M. Nießner, "ScanNet: Richly-annotated 3D Reconstructions of Indoor Scenes," Apr. 2017, arXiv:1702.04405. [Online]. Available: <http://arxiv.org/abs/1702.04405>
- [5] C. Choy, J. Gwak, and S. Savarese, "4D Spatio-Temporal ConvNets: Minkowski Convolutional Neural Networks," Jun. 2019, arXiv:1904.08755 [cs]. [Online]. Available: <http://arxiv.org/abs/1904.08755>
- [6] A. H. Lang, S. Vora, H. Caesar, L. Zhou, J. Yang, and O. Beijbom, "PointPillars: Fast Encoders for Object Detection from Point Clouds," Dec. 2018. [Online]. Available: <https://arxiv.org/abs/1812.05784v2>
- [7] B. Wu, X. Zhou, S. Zhao, X. Yue, and K. Keutzer, "SqueezeSegV2: Improved Model Structure and Unsupervised Domain Adaptation for Road-Object Segmentation from a LiDAR Point Cloud," in *2019 International Conference on Robotics and Automation (ICRA)*, May 2019, pp. 4376–4382, iSSN: 2577-087X. [Online]. Available: <https://ieeexplore.ieee.org/document/8793495>
- [8] Y. Wang, R. Ji, and S.-F. Chang, "Label Propagation from ImageNet to 3D Point Clouds."
- [9] A. Kundu, X. Yin, A. Fathi, D. Ross, B. Brewington, T. Funkhouser, and C. Pantofaru, "Virtual Multi-view Fusion for 3D Semantic Segmentation," A. Vedaldi, H. Bischof, T. Brox, and J.-M. Frahm, Eds., vol. 12369. Cham: Springer International Publishing, 2020, pp. 518–535, book Title: Computer Vision – ECCV 2020 Series Title: Lecture Notes in Computer Science. [Online]. Available: https://link.springer.com/10.1007/978-3-030-58586-0_31
- [10] J. McCormac, A. Handa, A. Davison, and S. Leutenegger, "SemanticFusion: Dense 3D Semantic Mapping with Convolutional Neural Networks," Sep. 2016, arXiv:1609.05130 [cs]. [Online]. Available: <http://arxiv.org/abs/1609.05130>
- [11] A. Caunes, T. Chateau, and V. Frémont, "3D Can Be Explored In 2D : Pseudo-Label Generation for LiDAR Point Clouds Using Sensor-Intensity-Based 2D Semantic Segmentation," in *2024 IEEE Intelligent Vehicles Symposium (IV)*, Jun. 2024, pp. 2192–2197, iSSN: 2642-7214. [Online]. Available: <https://ieeexplore.ieee.org/document/10588443>
- [12] D. Robert, B. Vallet, and L. Landrieu, "Learning Multi-View Aggregation In the Wild for Large-Scale 3D Semantic Segmentation," Jul. 2022, arXiv:2204.07548 [cs]. [Online]. Available: <http://arxiv.org/abs/2204.07548>
- [13] L. Ma, J. Stückler, C. Kerl, and D. Cremers, "Multi-View Deep Learning for Consistent Semantic Mapping with RGB-D Cameras," Dec. 2017, arXiv:1703.08866 [cs]. [Online]. Available: <http://arxiv.org/abs/1703.08866>
- [14] B. H. Wang, W.-L. Chao, Y. Wang, B. Hariharan, K. Q. Weinberger, and M. Campbell, "LDLS: 3-D Object Segmentation Through Label Diffusion From 2-D Images," *IEEE Robotics and Automation Letters*, vol. 4, no. 3, pp. 2902–2909, Jul. 2019, arXiv:1910.13955 [cs, eess]. [Online]. Available: <http://arxiv.org/abs/1910.13955>
- [15] H. Su, S. Maji, E. Kalogerakis, and E. Learned-Miller, "Multi-view Convolutional Neural Networks for 3D Shape Recognition," Sep. 2015, arXiv:1505.00880 [cs]. [Online]. Available: <http://arxiv.org/abs/1505.00880>
- [16] G. Neuhold, T. Ollmann, S. R. Buló, and P. Kotschieder, "The Mapillary Vistas Dataset for Semantic Understanding of Street Scenes," in *2017 IEEE International Conference on Computer Vision (ICCV)*. Venice: IEEE, Oct. 2017, pp. 5000–5009. [Online]. Available: <http://ieeexplore.ieee.org/document/8237796/>
- [17] H. Kim, Y. Kang, C. Oh, and K.-J. Yoon, "Single Domain Generalization for LiDAR Semantic Segmentation," in *2023 IEEE/CVF Conference on Computer Vision and Pattern Recognition (CVPR)*, Jun. 2023, pp. 17 587–17 598, iSSN: 2575-7075. [Online]. Available: <https://ieeexplore.ieee.org/document/10203512>
- [18] A. H. Gebrehiwot, D. Hurych, K. Zimmermann, P. Pérez, and T. Svoboda, "T-UDA: Temporal Unsupervised Domain Adaptation in Sequential Point Clouds," in *2023 IEEE/RSJ International Conference on Intelligent Robots and Systems (IROS)*, Oct. 2023, pp. 7643–7650, iSSN: 2153-0866. [Online]. Available: <https://ieeexplore.ieee.org/document/10341446>
- [19] A. Shaban, J. Lee, S. Jung, X. Meng, and B. Boots, "LiDAR-UDA: Self-ensembling Through Time for Unsupervised LiDAR Domain Adaptation," in *2023 IEEE/CVF International Conference on Computer Vision (ICCV)*, Oct. 2023, pp. 19 727–19 737, iSSN: 2380-7504. [Online]. Available: <https://ieeexplore.ieee.org/document/10377035>
- [20] H. Kim, Y. Kang, C. Oh, and K.-J. Yoon, "Single Domain Generalization for LiDAR Semantic Segmentation," in *2023 IEEE/CVF Conference on Computer Vision and Pattern Recognition (CVPR)*. Vancouver, BC, Canada: IEEE, Jun. 2023, pp. 17 587–17 598. [Online]. Available: <https://ieeexplore.ieee.org/document/10203512/>
- [21] J. Kim, J. Woo, J. Kim, and S. Im, "Rethinking LiDAR Domain Generalization: Single Source as Multiple Density Domains," Jul. 2024, arXiv:2312.12098 [cs]. [Online]. Available: <http://arxiv.org/abs/2312.12098>
- [22] J. Kim, J. Woo, U. Shin, J. Oh, and S. Im, "Density-aware Domain Generalization for LiDAR Semantic Segmentation," in *2024 IEEE/RSJ International Conference on Intelligent Robots and Systems (IROS)*, Oct. 2024, pp. 9573–9580, iSSN: 2153-0866. [Online]. Available: <https://ieeexplore.ieee.org/document/10801829>
- [23] J. Huang, "Neural Kernel Surface Reconstruction," Apr. 2023. [Online]. Available: <https://huangjh-pub.github.io>
- [24] B. Cheng, I. Misra, A. G. Schwing, A. Kirillov, and R. Girdhar, "Masked-attention Mask Transformer for Universal Image Segmentation," Jun. 2022, arXiv:2112.01527 [cs]. [Online]. Available: <http://arxiv.org/abs/2112.01527>
- [25] Z. Liu, Y. Lin, Y. Cao, H. Hu, Y. Wei, Z. Zhang, S. Lin, and B. Guo, "Swin Transformer: Hierarchical Vision Transformer using Shifted Windows," Aug. 2021, arXiv:2103.14030 [cs]. [Online]. Available: <http://arxiv.org/abs/2103.14030>
- [26] MMSegmentation Contributors, "OpenMMLab Semantic Segmentation Toolbox and Benchmark," Jul. 2020, original-date: 2020-06-14T04:32:33Z. [Online]. Available: <https://github.com/open-mmlab/mms Segmentation>
- [27] MMDetection3D Contributors, "OpenMMLab's Next-generation Platform for General 3D Object Detection," Jul. 2020, original-date: 2020-07-08T03:39:45Z. [Online]. Available: <https://github.com/open-mmlab/mmdetection3d>